Experimental and numerical study on eccentric compression properties of laminated bamboo columns with a chamfered section

Chaokun Hong[1a,1b,2], Haitao Li[1a,1b*], Zhenhua Xiong[3], Rodolfo Lorenzo[4], Ileana Corbi[5], Ottavia Corbi[5]

[1a] College of Civil Engineering, Nanjing Forestry University, Nanjing 210037, China; [1b] Joint International Research Laboratory of Bio-composite Building Materials and Structures, Nanjing Forestry University, Nanjing 210037, China.

[2] College of Civil Engineering and Architecture, Zhejiang University, Hangzhou 310058, China.

[3] Ganzhou Sentai bamboo company LTD, Ganzhou 341001, China.

[4] University College London, London WC1E 6BT, UK.

[5] University of Naples Federico II, Via Claudio 21,80133 Naples, Italy.

*Corresponding author: Haitao LI, Professor, E-mail: lhaitao1982@126.com

Abstract: The eccentric compression behavior of laminated bamboo lumber (LBL) columns with a chamfered section was investigated using eccentricity of 30mm, 60mm, 90mm and 120mm. The effect of eccentricity ratio on the ultimate bearing capacity, ultimate strain and failure mode was analyzed through eccentric compression tests. The failure modes of LBL columns with different eccentricities were basically same, which belonged to brittle tension failure. With the increase in eccentricity ratio, the ultimate bearing capacity and ultimate strain gradually decreased. The cross-section strain of the specimen was linearly distributed along the height direction, which conformed to the plane section assumption. The lateral deflection curves had similar characteristics under different load levels and could be expressed by sine half-wave curves. Based on the Hill failure criterion, a 3D finite element model was developed to calculate the ultimate bearing capacity of LBL columns with different dimensions under eccentric compression. According to the simulation results and test results, a general empirical formula was proposed considering both the influence of slenderness ratio and eccentricity ratio. The reliability of the proposed formula was verified by comparing the calculated results with the results in the existing literature.

Keywords: Laminated bamboo lumber; column; chamfer; eccentric compression; finite element model

1 Introduction

With the progress of times, the concept of sustainable development continues to gain popularity. Traditional building materials can cause greater pollution to the environment during production and utilization, therefore, research on the use of wood [1-3], bamboo [4-6] and other bio-based materials as alternative materials have gradually attracted widespread attention. Original bamboo has been used as structural components since ancient times because of its low-cost, rich resources and fast-growing features. However, due to the discrete mechanical properties, it cannot fully meet the requirements of contemporary life for building materials. Although in recent years, some scholars have conducted certain research on the improvement of raw bamboo materials [7-8], joint structure [9], dimension identification [10], and mechanical properties of composite structures [11], they still cannot solve this problem really well. Parallel bamboo strand

lumber (PBSL) [12-18], GluBam [19-21] and laminated bamboo lumber (LBL) [22-25] are currently three common types of engineered bamboo. Compared with original bamboo, their cross sections are dense and regular so that the dimensions are easy to be unified. Besides, the mechanical properties of engineered bamboo are comparable to those of engineered timber [26], which show a broad application prospects in the construction market.

Many researchers have carried out experimental investigation on the mechanical properties of LBL structural components. Luna et al. [27] investigated the axial compressive properties of LBL columns with square section. Li et al. [28-29] studied the eccentric compression performance of LBL columns with cross section sizes of 100 mm × 100 mm and 80 mm × 80 mm, and established empirical formulas for stability coefficient with eccentricity ratio and slenderness ratio as independent variable respectively; they also compared the mechanical properties of LBL columns under tangential and radial eccentric compression, and found that the ultimate bearing capacity and deformation results were basically same in the two directions. Karyadi et al. [30] studied the flexural performance of box-sectional LBL beam with wall thickness as an influencing factor. The results showed that the shear strength of the beam increased significantly with the increase in wall thickness, but the flexural elastic modulus didn't change significantly.

Research on the finite element analysis of LBL has also been carried out. Eratodi et al. [31] took the specific gravity G of material as the influencing factor and carried out experimental research and finite element analysis on the embedding strength of LBL. It was found that the embedding strength parallel to the grain direction of the specimen was significantly higher than that perpendicular to the grain direction. Khoshbakht et al. [32] evaluated the applicability of the testing method of dowel-bearing strength in ASTM D5764 standard for LBL. Three-dimensional bilinear finite element models for half-hole and full-hole were established. Based on Tsai-Wu failure criterion, the failure mechanism of half-hole and full-hole specimens was analyzed. Tang et al. [33] carried out an experimental study on the bolted connection of LBL, and comprehensively considered the influence of the thickness of laminated bamboo strips, end distance, bolt diameter and configuration of the bolts on the bearing capacity. The typical failure modes were summarized in the study, and based on the hill failure criterion, the ABAQUS finite element analysis was carried out which was in good agreement with the test results.

Actually, ideally axial compressed columns do not exist in the construction. For practical columns, the material itself inevitably exhibits inhomogeneity, and the resultant force acting on the column cannot coincide with the axis perfectly without any deviation. Eccentric compressive behavior of columns plays a key role in guaranteeing the overall stability of structures, thus the research on eccentric compression performance of LBL columns is significant to promote the utilization of engineered bamboo. In the current studies, researchers mainly focused on the structural members with square section, while it can be found in the existing engineering examples of LBL that some structural components have circular section or other special-shaped section (see Fig. 1) due to the requirements of appearance aesthetics [34]. Furthermore, the existing empirical

formulas proposed to calculate ultimate bearing capacity are insufficient, as mentioned before, the dimension and the cross-sectional shape of columns are limited, which can result in unreliable calculated results for other slenderness ratio. In terms of finite element analysis, most of the numerical studies are focused on the connection of LBL, and there is little literature for structural components like beams or columns. Therefore, it is necessary to carry out more research on finite element method for engineered bamboo.

Fig. 1(a) Lotus in Shenyu Island, China (b) Column with chamfered section in traditional timber structure

During the Ming and Qing Dynasties in China, columns with chamfered section (Fig. 1b) were commonly used in traditional timber structures. Compared with square-sectional columns, theirs shape is more varied and they are convenient to be fabricated. One of the applications of engineered bamboo is to make antique buildings. Therefore, LBL columns with a chamfered section were chosen to carried out eccentric compression tests in this paper. The finite element analyses were carried out to calculate ultimate bearing capacity of LBL columns with different dimension by using Hill failure criterion. The experimental and numerical results were compared and analyzed to verify each other firstly. Then based on the test results and simulation results, a general empirical formula was proposed considering both the influence of slenderness ratio and eccentricity ratio. The proposed formula was furtherly verified by comparing the calculated results with existing literature and simulation results of circular-sectional column. The work in this paper can provide reliable test data and simulation analysis method for the further promotion and application of laminated bamboo lumber.

2 Test setup

2.1 Design and fabrication of LBL columns

In this paper, LBL columns were all produced in Ganzhou city, China. With moso bamboo from Yongan, Fujian as raw material and resorcinol as adhesive, under the pressure of 9 MPa for upper and lower surfaces and 6.5 MPa for the left and right surfaces, bamboo laminates were hot pressed together in 157℃ condition for about 15 minutes. The arrangement of bamboo laminates and the cross-sectional shape of LBL columns are shown in Fig. 2. To satisfy the length demand

in longitudinal direction, bamboo laminates were connected by mechanical connection (Fig. 3). The moisture content and density of LBL in the test were 7.0% and 736kg/m^3 respectively.

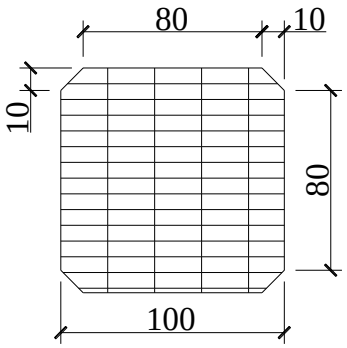

Fig. 2 Cross section of LBL column and arrangement of bamboo laminates

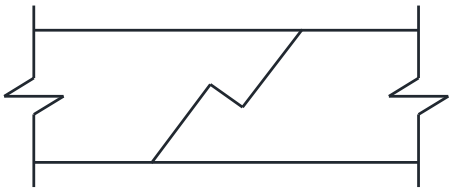

Fig. 3 Mechanical connection

To the authors' knowledge, the cross section and length of LBL columns used in the existing engineering examples usually vary from 100 mm × 100 mm~300 mm × 300 mm and 3 m ~ 4 m respectively. They are related to slenderness ratios of 34.64~138.56. Due to the limitation of the test site, the dimension of 100 mm × 100 mm × 1100 mm (slenderness ratio of 38.75) was chosen in this study. Considering the influence of eccentricity, 5 groups of LBL columns were designed with 3 replicates in each group. One group was for axial compression test with the eccentricity of 0 mm, and the eccentricity in the other 4 groups was set as 30 mm, 60 mm, 90 mm and 120 mm successively. The width b and height h of cross section were both 100mm, and the four corners were chamfered with a dimension of 10mm. According to the reference [28], it was found that the ultimate bearing capacity and deformation results were basically same in the radial and tangential direction, while more crack layers appeared for radial eccentric direction group specimens due to the layer structure. Therefore, the tangential eccentric direction was chosen in this study (Fig. 4a).

The cross section and dimension of brackets are shown in Fig. 4b, and the assembly diagram of LBL columns with brackets is shown in Fig. 4c. The bamboo brackets and bamboo columns were connected by six steel bolts and structural adhesive. To guarantee the eccentric effect, the thickness of brackets was both 50 mm in Group E30 and E60, while for Group E90 and E120, the thickness of brackets was 100 mm and 150mm respectively. More detailed parameters of specimens are summarized in Table 1. All the columns took the wide surface of the bamboo strip as side A, and marked the remaining surfaces as side B, C and D successively along the counterclockwise direction. The top surface was denoted with ∗ and the bottom surface was blank.

Table 1 Detailed parameters of specimens

Group	Length	Slenderness ratio	Number	Eccentricity	Bracket thickness	Bracket height
E0			3	0	—	—
E30			3	30	50	260
E60	1100mm	38.75	3	60	50	260
E90			3	90	100	260
E120			3	120	150	260

Note: The top and bottom ends were unidirectional hinge supports, so the effective length to define slenderness ratio was equal to the column length.

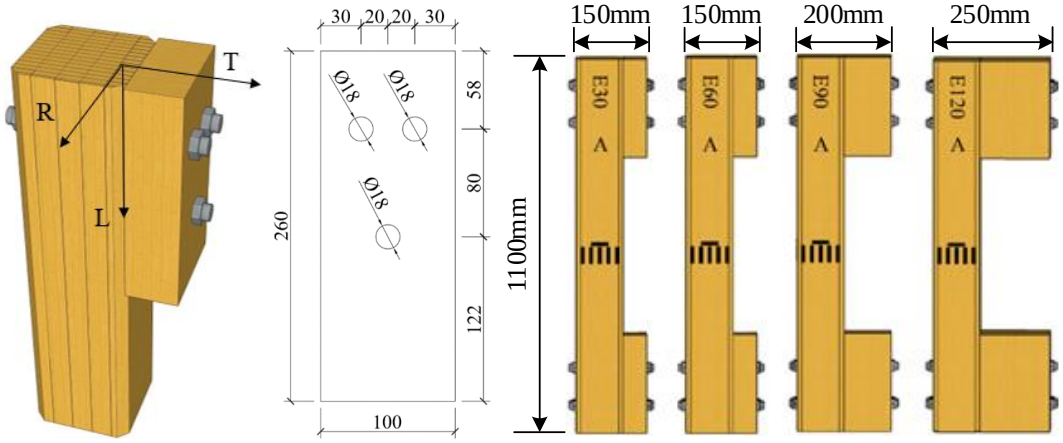

Fig. 4 (a) Tangential eccentric direction (b) Cross section and dimension of bracket (c) Dimension of columns

2.2 Test loading system

According to the standard for test methods of timber structures (GB/T 50329-2012), the loading system was designed. The physical and schematic diagram of the test are shown in Fig. 5. The upper and lower ends were unidirectional hinge supports to ensure the specimen can only rotate freely in the eccentric direction and avoid accidental deformation outside the eccentric plane. A 100t microcomputer controlled electro-hydraulic servo universal testing machine was selected for the test. TDS-540 data acquisition instrument was used for data collection. Load control was adopted in the initial stage of loading, and displacement control was used when the load reached 80% of the ultimate load. The time from loading to failure was controlled within 5~10 min. The tests were completed in the structural laboratory of Nanjing Forestry University.

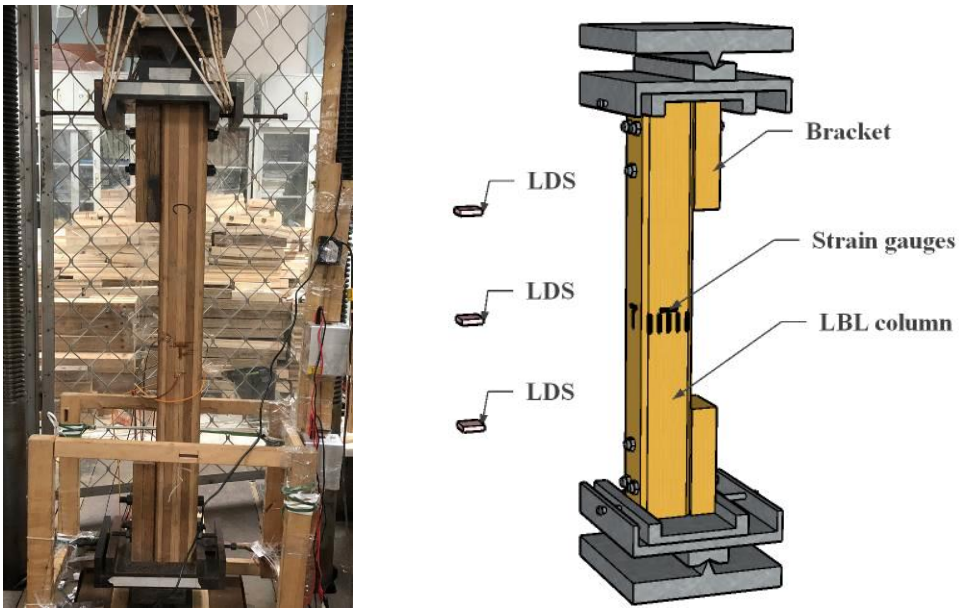

Fig. 5 (a) Eccentric compression test (b) Schematic diagram of test

2.3 Arrangement of test points

The measurement contents included lateral and longitudinal strain in the center of column,

lateral deflection at the quarter point along the column, axial displacement of column and ultimate load. Lateral and vertical strain gauges were pasted on four side surfaces in the midspan. One lateral strain gauge and one vertical strain gauge were pasted on B, C and D surface. As for A surface, in addition to a lateral strain gauge, five vertical strain gauges were pasted along the height direction of section. The arrangement of strain gauges is shown in Fig. 6. The size of strain gauges was 20 mm × 3 mm. The lateral deflection at the quarter point were measured by three laser displacement sensors, which were one-to-one corresponding to the quarter points of the real object during loading process. The axial displacement was measured by a displacement meter.

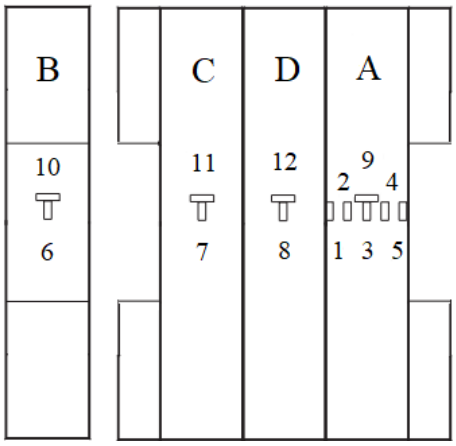

Fig. 6 Arrangement of strain gauges

3 Test results and analysis

3.1 Failure mode and mechanism analysis

At the beginning of the test, the strain, axial deformation and lateral deflection data of each point increased linearly, but no significant deformation could be observed from the appearance. With the continuous increase in load, the specimen entered the yield stage. The stress at the edge of compression zone exceeded proportional limit strength of the material, and the bending extent of column became more significant. At the end of the test, the increasing rate of reaction force gradually decreased, while the lateral deflection continuously increased until the outermost bamboo laminates on tensile side were broken (Fig. 7).

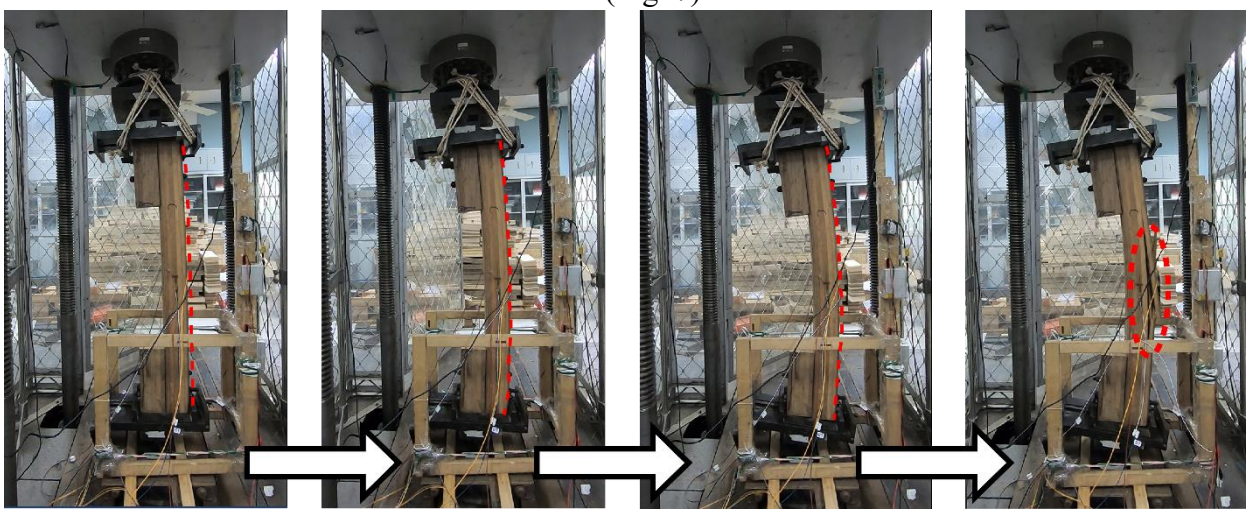

Fig. 7 Failure process of E90-1

The failure modes of columns with different eccentricities were basically consistent, which belonged to brittle tension failure (Fig. 8, the position of red circles is the center of column). In addition to the expectant cracks occurring in the central part of columns on tensile side, the other cracking positions randomly occurred along the column due to two defects, namely original bamboo node and the finger joint (Fig. 9). The finger joint is used to extend the length of bamboo laminates to form a longer structural component. At present, the extension of bamboo laminates mainly depends on manual splicing, so there are always some small gaps occuring in the LBL components, which are the weakest area except for bamboo nodes. Under the condition of eccentric compression, the bamboo laminates on tensile side are much easier to crack at the position of bamboo nodes and finger joints.

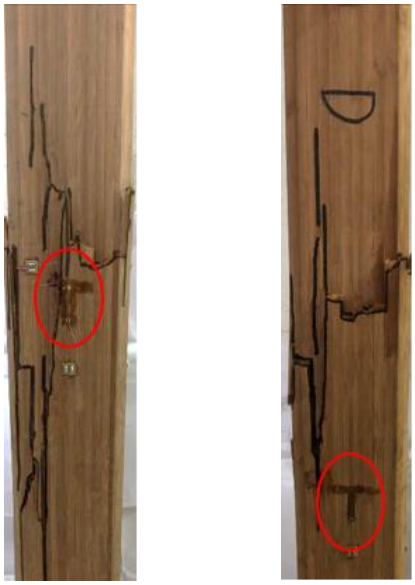

Fig .8 Cracking position (a) near the center (b) far from center

Bamboo node effect on tensile properties of laminated bamboo has been studied in the reference [35]. The results showed that the number of bamboo nodes significantly affected the tensile properties in parallel-to-grain direction. Thus, there is no doubt that people may confuse about the location effect of bamboo nodes and finger joints in the real objects. Although the two factors are randomly distributed in LBL component, from the perspective of overall structural performance, the difference of mechanical properties could be negligible (Table 2). The two factors could be considered as only affecting the initial cracking position.

（a）Finger joint （b）Bamboo node

Fig. 9 Two key factors affecting damage

3.2 Main test results

Measured ultimate load of the columns subjected to axial compression were 447.83 kN, 385.25 kN and 495.08 kN respectively; the variation coefficient of ultimate load was 10% and the average ultimate strength was 45.18 MPa. Main test results of the columns under eccentric compression are shown in Table 2. Where P_{max} is ultimate load; S_{ul} is ultimate axial deformation; w_{ul} is ultimate midspan lateral deflection; ε_{uasA} and ε_{ulsA} are ultimate longitudinal strain and lateral strain on surface A respectively; ε_{uasB}, ε_{ulsB}, ε_{uasD} and ε_{ulsD} are corresponding ultimate strain on surface B and D. The strain values and change law on surface C were close to that of surface A, so it is no longer presented in the table.

Table 2 Main test results

Group		P_{max} /kN	w_{ul} /mm	ε_{uasA} / $\mu\varepsilon$	ε_{ulsA} / $\mu\varepsilon$	ε_{uasB} / $\mu\varepsilon$	ε_{ulsB} / $\mu\varepsilon$	ε_{uasD} / $\mu\varepsilon$	ε_{ulsD} / $\mu\varepsilon$
E30	Mean	128.89	42.87	-3588	981	-16611	4395	9505	-2173
	COV	2.66%	15.77%	22.07%	40.46%	11.86%	8.46%	11.12%	12.05%
E60	Mean	94.81	52.04	-2692	974	-14527	4020	9502	-2256
	COV	2.17%	7.44%	31.14%	42.69%	7.89%	6.50%	8.78%	20.35%
E90	Mean	72.79	37.64	-2235	539	-14082	2870	8502	-2409
	COV	3.14%	6.79%	6.73%	56.24%	5.13%	6.35%	3.58%	6.60%
E120	Mean	55.71	33.44	-1559	604	-10888	3221	8030	-2278
	COV	1.99%	9.41%	48.13%	16.76%	8.77%	4.32%	5.89%	6.78%

Note: COV means coefficient of variation; $\mu\varepsilon$ is micro strain.

The variation coefficients of ultimate load and ultimate midspan deflection are both within 20%, which means the test results are reliable. The variation coefficients of some ultimate strain values are more than 20%. The reason is that some bamboo laminates crack layer by layer at the tensile side before column reaches the ultimate load, and the extreme deformation during cracking leads to inaccurate strain values.

It is stipulated in GB 50005-2017 that the maximum deflection of flexural member should not exceed 1/250 of the span. For the specimens with a span of 1100 mm, the allowable deflection should not exceed 4.4 mm. The test results show that the ultimate midspan deflection corresponding to the ultimate load is far greater than 4.4 mm regardless of eccentricity, which indicates that deformation or stiffness should be carefully controlled in the design of LBL columns.

3.3 Load vs displacement curves

Fig. 10 shows load vs midspan deflection curves and load vs axial deformation curves of specimens with different eccentricity. In the initial stage of test, the midspan deflection and the axial deformation increased linearly with the increase in load. After entering the nonlinear phase, the slope of curves began to decrease. At this stage, a small amount of dislocation occurred between bracket and column because of the damage of structural adhesive, which resulted in a

slight decrease in reaction force and midspan deflection. However, the column was not broken and the steel bolts could still bear the load, so the specimen appeared the strengthening of bearing capacity after partial failure. After reaching the ultimate load, bamboo laminates on the tensile side cracked and the column was destroyed. The bearing capacity of specimen was lost, and the test was terminated.

It can be seen from the figure that with the increase in eccentricity, the stiffness and the ultimate load of specimen gradually decreased, while the ultimate midspan deflection and ultimate axial deformation showed a trend of first increasing and then decreasing.

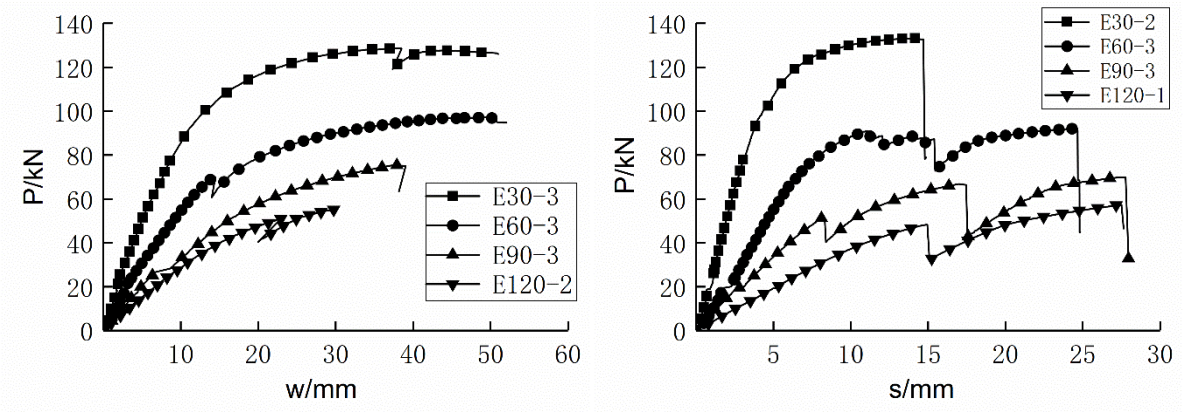

（a）Load vs midspan deflection curves （b）Load vs axial deformation curves

Fig. 10 Load vs displacement curves

3.4 Load vs strain curves

Figs. 11 to 12 are load vs axial strain curves and load vs lateral strain curves, respectively, in which tensile strain is positive and compressive strain is negative. At the beginning of test, there was a linear relationship between strain and load. As the load increased, the compression zone of section gradually yielded and entered the plastic deformation stage. The increasing rate of load slowed down, while that of strain accelerated.

Surface B of all the specimens was under compression in the length direction, and the longitudinal and lateral strain values of Surface B were larger than the other three surfaces. Surface D of all the specimens was under tension in the length direction. The strain values of Surface A and Surface C were basically coincident. With the increase in the eccentricity, the increasing rate of strain on the Surface B and Surface D gradually increased, but the strain values on the surface A and surface C gradually decreased.

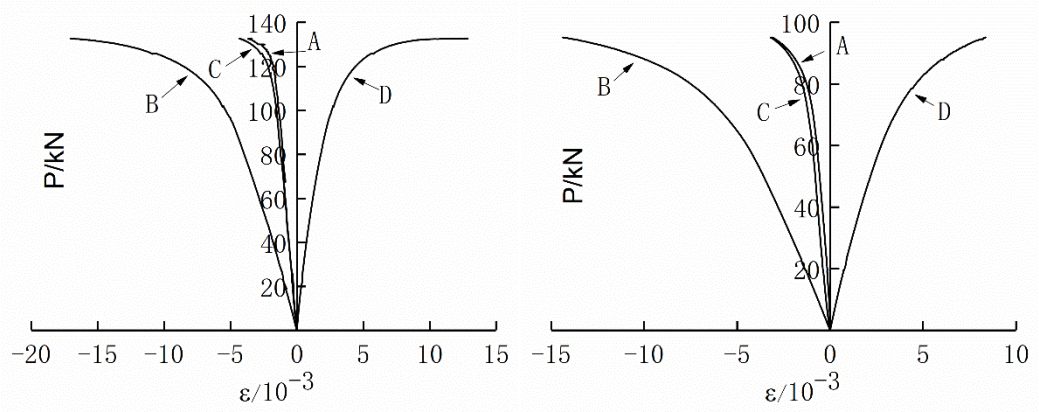

（a）E30-2　　（b）E60-2

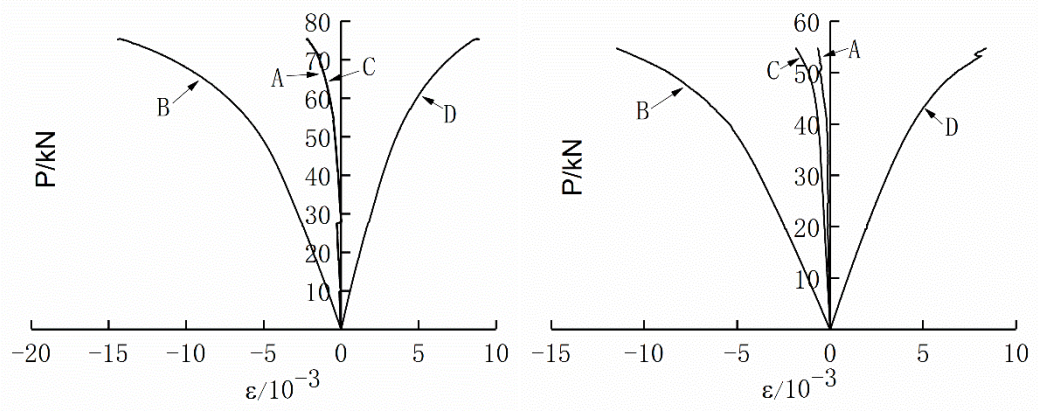

（c）E90-3　　（d）E120-1

Fig. 11 Load vs longitudinal strain curves

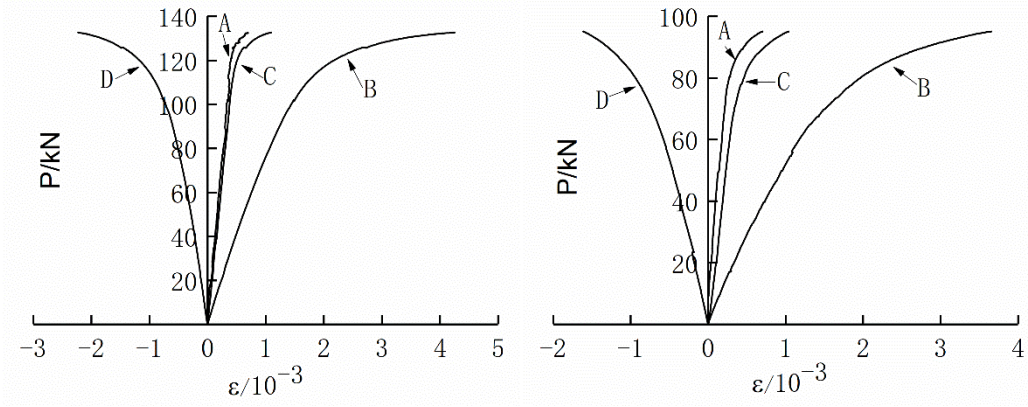

（a）E30-2　　（b）E60-2

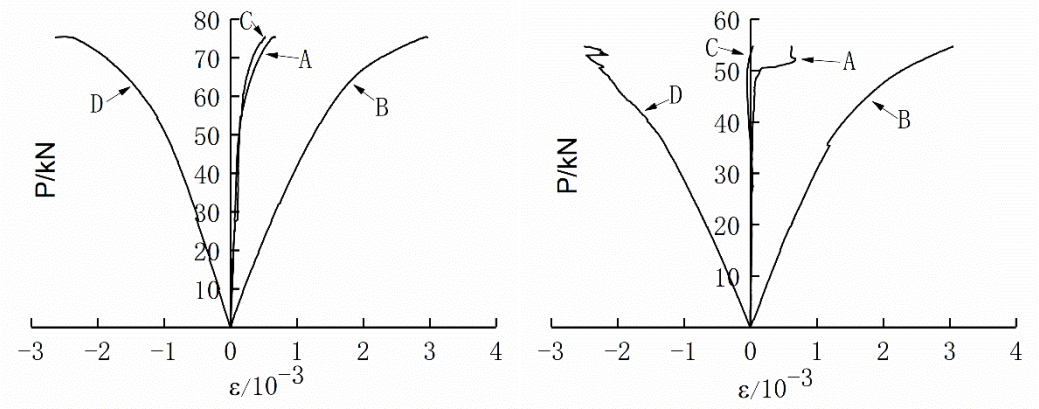

（c）E90-3　　（d）E120-1

Fig. 12 Load vs lateral strain curves

3.5 Lateral deflection curves under different load level

Figure 13 shows the lateral deflection curves of specimens under different load level. It can be seen from the figures that regardless of the load level and eccentricity, the lateral deformation curves had similar characteristics. As the eccentricity increased, the amplitude of lateral deflection gradually increased. For LBL columns with hinge supports at both ends, the shape of lateral deflection curves were close to that of sine function curve, which could be expressed by Equation (1):

$$w = w_m \sin\frac{\pi H}{L} \tag{1}$$

where w is the lateral deflection of LBL column at any position under different load level; w_m is the midspan lateral deflection; H is the distance from any point to the bottom of column; L is the length of column.

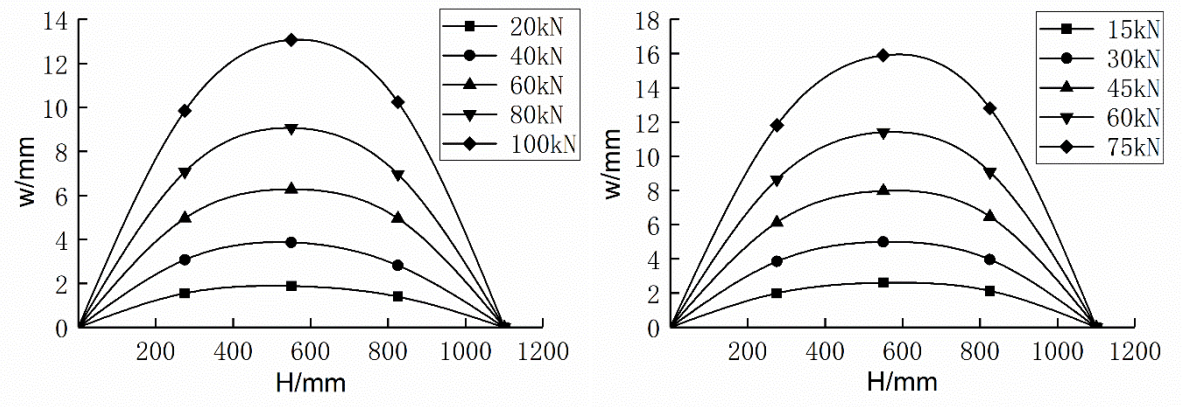

（a）E30-3　　（b）E60-1

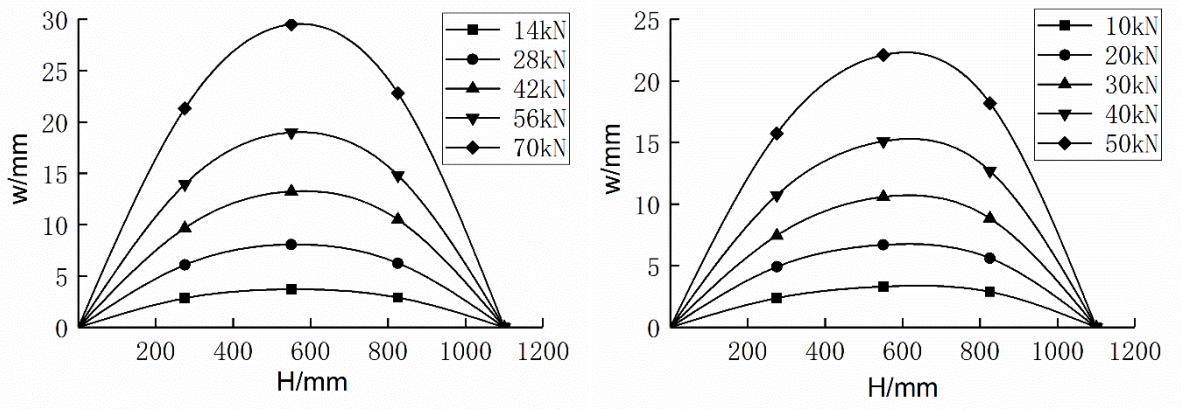

（c）E90-2　　（d）E120-2

Fig. 13 Lateral deflection curves

3.6 Verification of plane section assumption

Fig. 14 shows the variation of longitudinal strain along the height direction of section under different load level. During the loading process, the distribution of longitudinal strain basically maintained a linear proportional relationship, indicating that the original section of LBL column still remained a plane after bending, which conformed to the plane section assumption.

The position where the strain value was 0 was between 30mm and 50mm, which meant that the position of neutral axis of column under eccentric compression was biased to the tensile side. With the increase in load, the neutral axis gradually moved to deeper area of tensile side. Due to the fact that the compressive strength of LBL is smaller than tensile strength, the neutral axis must move to tensile side to ensure the balance of stress on section when compression zone enters plastic deformation stage.

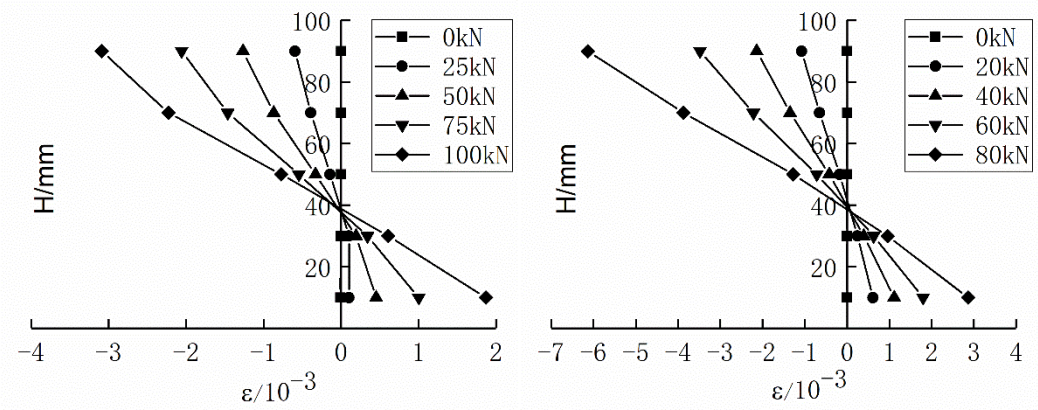

（a）E30-1　　（b）E60-2

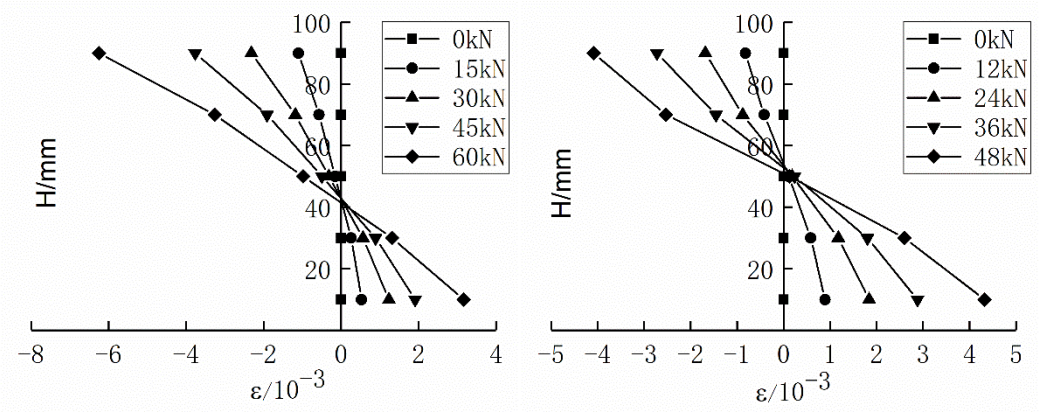

（c）E90-1　　（d）E120-2

Fig. 14 Verification of plane section assumption

3.7 Correlation between test results and eccentricity ratio

Fig. 15 shows the correlation between the strain of Surface B, D and eccentricity ratio, where the eccentricity ratio is e_0 / h. Compared with lateral strain, the dispersion of ultimate longitudinal strain was relatively small. With the increase in eccentricity ratio, the ultimate longitudinal strain values gradually decreased, while the ultimate lateral strain values generally showed a downward trend.

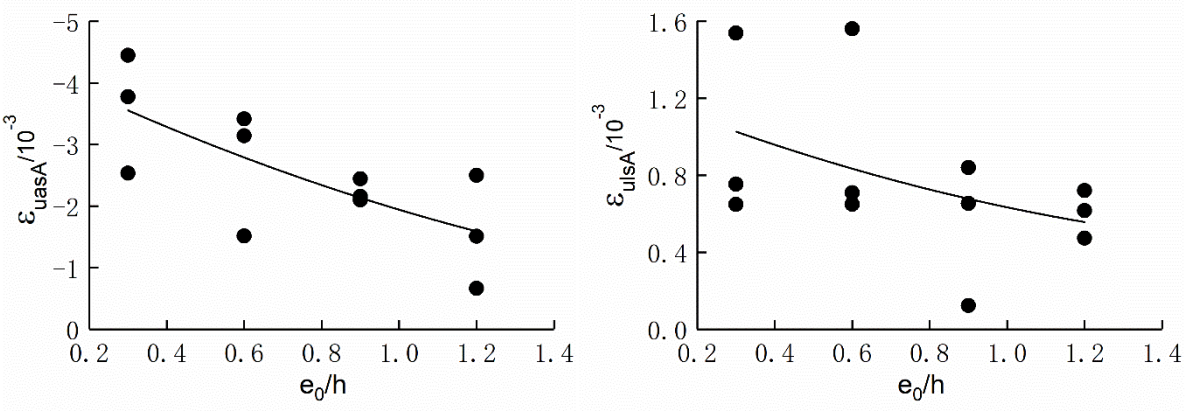

(a) Longitudinal strain on surface A　　(b) Lateral strain on surface A

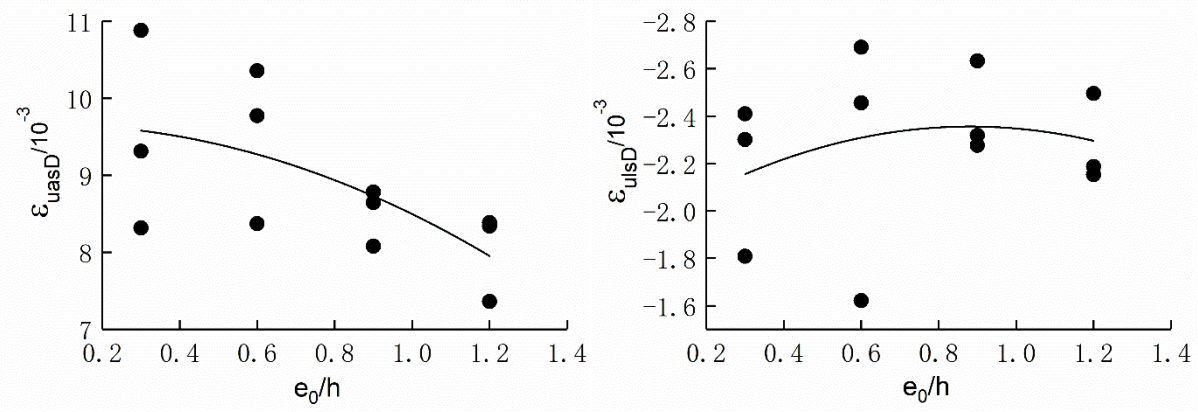

(c) Longitudinal strain on surface D　　(d) Lateral strain on surface D

Fig. 15 Correlation between ultimate strain and eccentricity ratio

Fig. 16 shows the correlation between the ultimate axial deformation, the ultimate midspan deflection and eccentricity ratio. It can be seen that as the eccentricity ratio of specimen increased, the ultimate displacement showed a trend of first increasing and then decreasing.

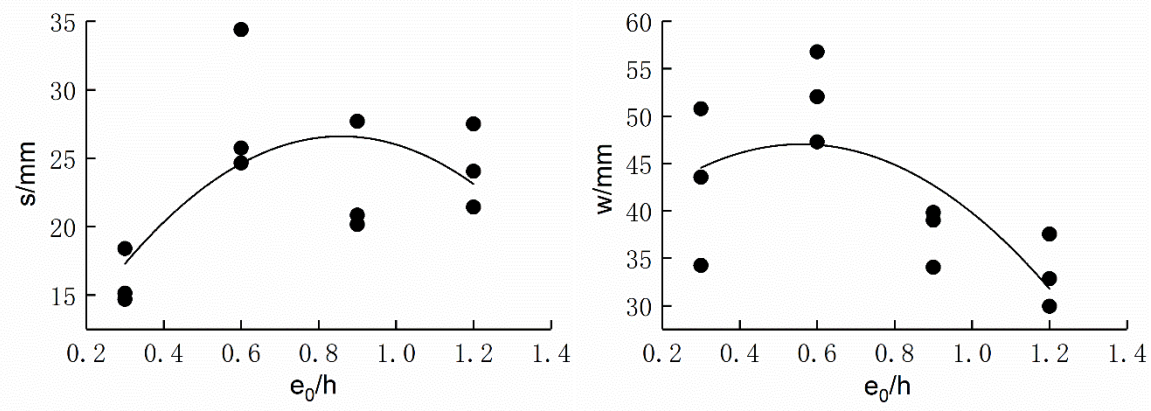

（a）Axial deformation （b）Midspan deflection

Fig. 16 Correlation between ultimate displacement and eccentricity ratio

Through regression analysis, the relationship between ultimate displacement and eccentricity ratio can be expressed by Equation (2) and (3):

$$S_{ul} = 4.6 + 51.3(e_0 / h) - 29.9(e_0 / h)^2 \tag{2}$$

$$w_{ul} = 35.4 + 41.5(e_0 / h) - 37.1(e_0 / h)^2 \tag{3}$$

where S_{ul} is the ultimate axial deformation, w_{ul} is the ultimate midspan deflection.

Fig. 17 shows the relationship between the ultimate load and eccentricity ratio. The ultimate load decreased with the increase in eccentricity ratio. The relationship between the ultimate load and eccentricity ratio can be expressed by formula (4):

$$P_{ul} = 47.21(e_0 / h)^2 - 151.34(e_0 / h) + 169.69 \tag{4}$$

where P_{ul} is the ultimate load.

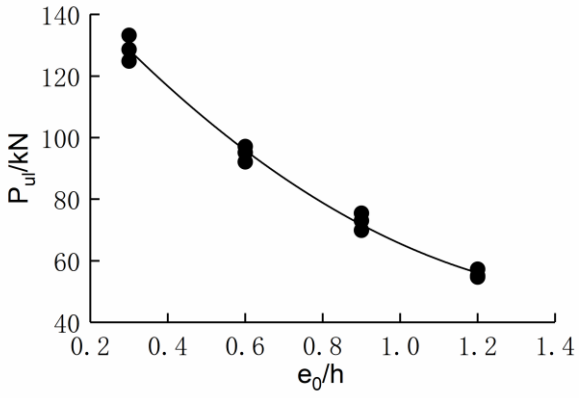

Fig. 17 Correlation between ultimate load and eccentricity ratio

4 Evaluation of ultimate bearing capacity for LBL columns

4.1 Existing calculation formulas for eccentric compression

Researchers have already done a large amount of experimental research on the mechanical properties of square-sectional LBL columns under eccentric compression, and established ultimate bearing capacity formulas based on the test data. To verify the universality of these existing formulas, the calculation results are listed in Table 3 and compared with the test data in this paper.

In general, the ultimate bearing capacity is calculated by:

$$N = \varphi f_c A \tag{5}$$

where φ is stability factor, f_c is compressive strength, A is cross-sectional area.

Li et al. [28-29] proposed empirical Equations. (6) ~ (7) to calculate the ultimate bearing capacity of LBL columns under eccentric compression:

$$\varphi_e = \frac{1}{1.73 + 4.14 e_0 / h} \tag{6}$$

$$\varphi_\lambda = \frac{1}{0.029\lambda - 0.0638} \tag{7}$$

where φ_e and φ_λ are stability factor, e_0 is eccentricity, h is the height of cross section, λ is slenderness ratio.

As can be seen in Table 3, the results of Equation (6) are close to the test results, because the sizes of specimen in two studies are similar. Equation (7) cannot be used for the calculation, since the formula was established with slenderness ratio as independent variable under the condition of eccentricity of 37mm. Although the existing formulas have a certain degree of guiding significance and clearly describe the relationship between ultimate bearing capacity and impact factors, they are not universal enough. Equations (6) ~ (7) are limited as they only use eccentricity ratio or slenderness ratio as independent variable respectively, so there will be a great error once the length or cross-sectional shape (i.e. slenderness ratio) of column changes. Also, they cannot be used to calculate ultimate load for LBL columns under axial compression.

Therefore, a 3D finite element model (FEM) was developed to calculate the ultimate bearing capacity of LBL columns under eccentric compression. Furtherly, a more general empirical formula was established based on the test and simulation results.

Table 3 Comparison of formulas and calculation results

Literature	0.3	0.6	0.9	1.2
Test results/kN	128.89	94.81	72.79	55.71
Li et al. [28]/kN	148.86	105.06	81.14	66.10
Error/%	15.49	10.81	11.47	18.65
Li et al. [29]/kN	—	—	—	—

Note: Error = (Calculation-test) / test ×100%.

4.2 Finite element analysis

4.2.1 Constitutive model and failure criterion

Laminated bamboo lumber is a typical anisotropic material, and it has obvious strain hardening behavior under compression (Fig. 18a). However, the aim of this study is to obtain the ultimate bearing capacity of LBL columns. ABAQUS subroutine was used to perform finite element analysis, so the material was simplified as an orthotropic material for the sake of reducing complexity of the codes. The constitutive model used is shown in Fig. 18b, where X_t and X_c are the tensile strength and compressive strength of LBL along the grain direction (L), Y_t and Y_c are the tensile strength and compressive strength along the radial direction (R), Z_t and Z_c are the tensile strength and compressive strength along the tangential direction (T), respectively.

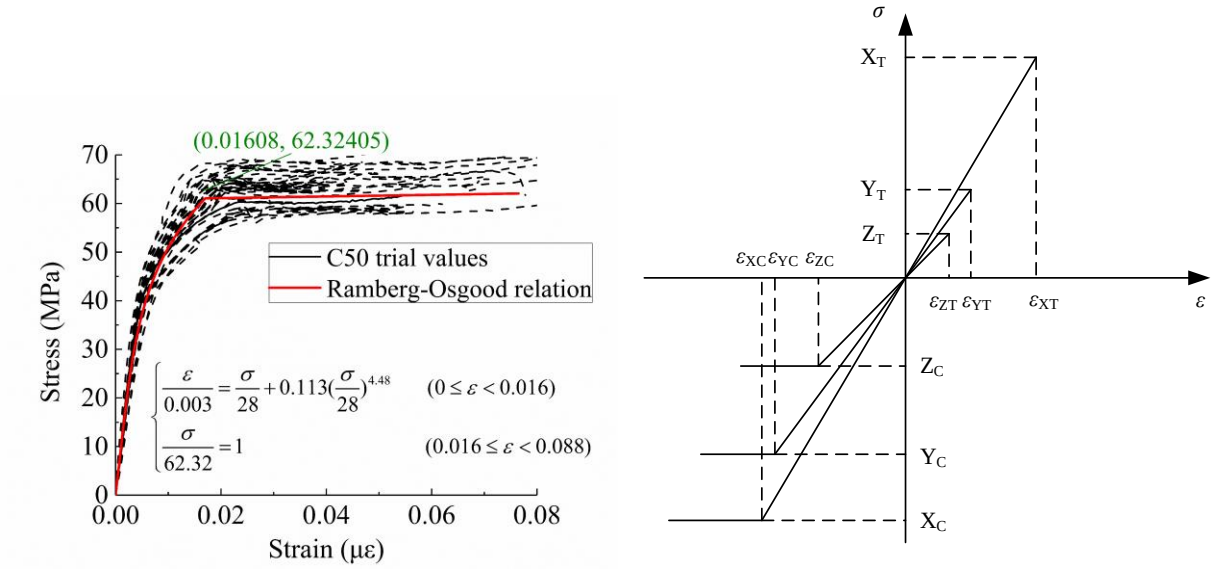

(a) Real stress-strain behavior [36] (b) Ideal elastoplastic behavior

Fig. 18 Constitutive model of LBL

The stress-strain relationship in elastic phase can be expressed by equation (8):

$$\begin{bmatrix}\sigma_{11}\\ \sigma_{22}\\ \sigma_{33}\\ \sigma_{12}\\ \sigma_{23}\\ \sigma_{31}\end{bmatrix}=\begin{bmatrix}D_{1111} & D_{1122} & D_{1133} & 0 & 0 & 0\\ D_{1122} & D_{2222} & D_{2233} & 0 & 0 & 0\\ D_{1133} & D_{2233} & D_{3333} & 0 & 0 & 0\\ 0 & 0 & 0 & D_{1212} & 0 & 0\\ 0 & 0 & 0 & 0 & D_{2323} & 0\\ 0 & 0 & 0 & 0 & 0 & D_{3131}\end{bmatrix}\begin{bmatrix}\varepsilon_{11}\\ \varepsilon_{22}\\ \varepsilon_{33}\\ \varepsilon_{12}\\ \varepsilon_{23}\\ \varepsilon_{31}\end{bmatrix} \tag{8}$$

where $D_{1111}=E_1(1-v_{23}v_{32})\gamma$, $D_{2222}=E_2(1-v_{13}v_{31})\gamma$, $D_{3333}=E_3(1-v_{12}v_{21})\gamma$, $D_{1122}=E_1(v_{21}+v_{31}v_{23})\gamma$, $D_{1133}=E_3(v_{13}+v_{12}v_{23})\gamma$, $D_{2233}=E_2(v_{32}+v_{12}v_{31})\gamma$, $D_{1212}=2G_{12}$, $D_{3131}=2G_{31}$, $D_{2323}=2G_{23}$, $\varepsilon_{12}=\gamma_{12}/2$, $\varepsilon_{23}=\gamma_{23}/2$, $\varepsilon_{31}=\gamma_{31}/2$, $\gamma=(1-v_{12}v_{21}-v_{23}v_{32}-v_{31}v_{13}-2v_{21}v_{32}v_{13})^{-1}$。

E_1, E_2, and E_3 are elastic modulus in the L, T and R direction respectively; G_{12}, G_{31} and G_{23} are shear modulus in L-T, L-R and R-T plane respectively; v_{ij} are Poisson's ratio; σ_{ij} and ε_{ij} are stress and strain respectively. According to authors' previous work [37], the constitutive model parameters are shown in Table 4, and the Hill failure criterion [38] was chosen for finite

element analysis:

$$F(\sigma_{ij})=\sqrt{\begin{matrix}F\left(\sigma_{22}-\sigma_{33}\right)^2+G\left(\sigma_{33}-\sigma_{11}\right)^2+H\left(\sigma_{11}-\sigma_{22}\right)^2\\+2L\sigma_{23}^2+2M\sigma_{31}^2+2N\sigma_{12}^2\end{matrix}} \tag{9}$$

where F, G, H, L, M, N are constants determined by the strength of material, which can be calculated by formulas (10)~(15):

$$F=\frac{\left(\sigma^0\right)^2}{2}\left(\frac{1}{\bar{\sigma}_{22}^2}+\frac{1}{\bar{\sigma}_{33}^2}-\frac{1}{\bar{\sigma}_{11}^2}\right)=\frac{1}{2}\left(\frac{1}{R_{22}^2}+\frac{1}{R_{33}^2}-\frac{1}{R_{11}^2}\right) \tag{10}$$

$$G=\frac{\left(\sigma^0\right)^2}{2}\left(\frac{1}{\bar{\sigma}_{33}^2}+\frac{1}{\bar{\sigma}_{11}^2}-\frac{1}{\bar{\sigma}_{22}^2}\right)=\frac{1}{2}\left(\frac{1}{R_{33}^2}+\frac{1}{R_{11}^2}-\frac{1}{R_{22}^2}\right) \tag{11}$$

$$H=\frac{\left(\sigma^0\right)^2}{2}\left(\frac{1}{\bar{\sigma}_{11}^2}+\frac{1}{\bar{\sigma}_{22}^2}-\frac{1}{\bar{\sigma}_{33}^2}\right)=\frac{1}{2}\left(\frac{1}{R_{11}^2}+\frac{1}{R_{22}^2}-\frac{1}{R_{33}^2}\right) \tag{12}$$

$$L=\frac{1}{2}\left(\frac{\tau^0}{\bar{\sigma}_{23}^2}\right)^2=\frac{3}{2R_{23}^2} \tag{13}$$

$$M=\frac{1}{2}\left(\frac{\tau^0}{\bar{\sigma}_{13}^2}\right)^2=\frac{3}{2R_{13}^2} \tag{14}$$

$$N=\frac{1}{2}\left(\frac{\tau^0}{\bar{\sigma}_{12}^2}\right)^2=\frac{3}{2R_{12}^2} \tag{15}$$

where $\bar{\sigma}_{ii}$ are material strength in the three directions, $\bar{\sigma}_{ij}$ are shear strength, σ^0 is reference yielding stress. R_{ij} can be calculated by equations (16):

$$R_{11}=\frac{\bar{\sigma}_{11}}{\sigma^0},R_{22}=\frac{\bar{\sigma}_{22}}{\sigma^0},R_{33}=\frac{\bar{\sigma}_{33}}{\sigma^0},R_{12}=\frac{\bar{\sigma}_{12}}{\tau^0},R_{13}=\frac{\bar{\sigma}_{13}}{\tau^0},R_{23}=\frac{\bar{\sigma}_{23}}{\tau^0} \tag{16}$$

Table 4 Constitutive model parameters

Elastic modulus（MPa）		Poisson's ratio		Strength（MPa）			
E1	6323.7	μ12	0.25	X_T	98	S_{XY}	18.13
E2	1468.53	μ21	0.054	Xc	59.63	S_{YZ}	22.59
E3	1192.06	μ13	0.2	Y_T	8.26	S_{ZX}	6.58
G12	1365.08	μ31	0.04	Y_C	21.91	σ^0	59.63
G23	461.81	μ23	0.43	Z_T	8.26		
G13	1260.09	μ32	0.435	Z_C	19.85		

4.2.2 Modeling details

As shown in Fig. 19, the models of bamboo bracket and bamboo column were created. The numerical model ignored the imperfection of laminated bamboo and the influence from structural adhesive and steel bolts. The contact surfaces between bracket and column were tied together.

Reference points (RP) were created for the model to apply load and constrains. Two RPs were created on the top and bottom surface respectively. With these RPs, the coupled constrains were set to apply the displacement-controlled loads. The upper and lower ends were unidirectional hinge supports to ensure the specimen can only rotate freely in the eccentric direction, therefore, U1, U2, U3, UR1, UR3 were restrained on the both ends. The type of solid elements was Explicit/C3D8R and the meshing density was 10 (approximate global size). In order to ensure that the kinetic energy was less than 10% of the strain energy and met the conditions of quasi-static analysis, the calculation step was set to 1s, and the displacement-controlled loads were loaded through the smooth analysis step.

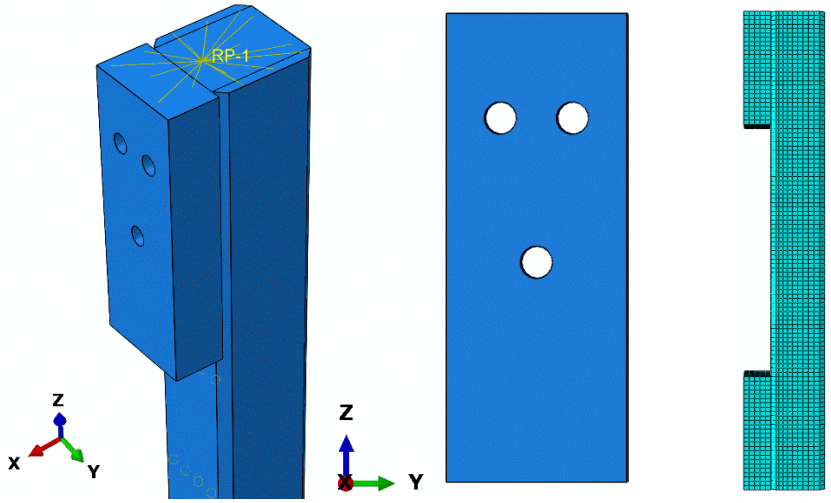

(a) LBL column (b) Bracket (c) Mesh

Fig. 19 Finite element model of laminated bamboo column

4.2.3 Basis of element deletion

According to the test results, the failure mode of eccentric compression columns was brittle tension failure along the grain direction. Therefore, in the following finite element analysis, the judgment of whether the elements are deleted or not is based on the stress σ_{11} along the grain direction. First, substitute the calculated trial stress into the failure criterion to judge whether it yields or not. If there is no yield, the stress integration point is in the linear elastic stage. At this time, the real stress in the program is equal to the trial stress, and the trial stress value is assigned to the state variable stressNew as the stressOld for the next calculation. If it yields, the stress integration point is in the plastic stage. If $\sigma_{11} < 0$, the element is under compression along the grain direction. The stress needs to be pulled back to the yield surface, and this point enters the state of plastic flow. If $\sigma_{11} > 0$, the element is under tension along the grain direction. Then the element is judged to be deleted. Because the numerical model ignored the imperfection of the laminated bamboo, in order to properly consider the effect of the imperfection, the average ultimate strength (45.18 MPa) of axially loaded columns was used as the yield value for $F(\sigma_{ij})$.

4.2.4 Validation of the finite element model

Take E30 as an example to discuss. At first, E30 was uniformly compressed in the initial

stage, the midspan deflection and axial deformation increased linearly with the increase in load. With the further increase in load, the specimen gradually entered the yield stage. The increasing rate of load slowed down, while the increase in midspan deflection and axial deformation accelerated significantly. Then the ultimate stress state reached the failure criterion standard, the tensile side cracked and the specimen lost the bearing capacity. The comparison deformation is shown in Fig. 20.

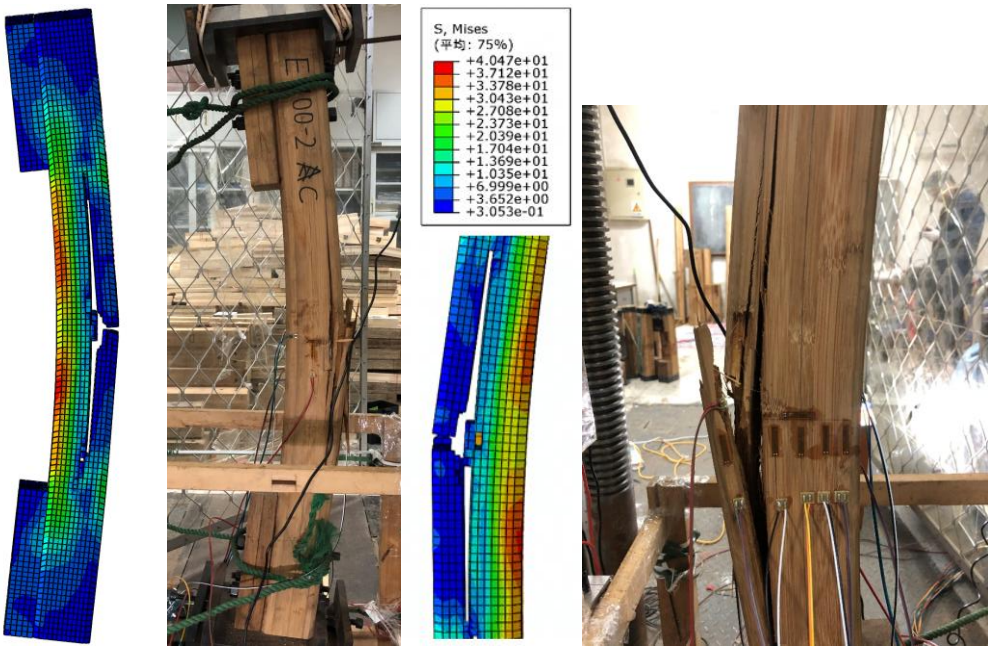

(a) Cracking simulation (b) E30-2 (c) Simulated local result (d) E30-2 local result

Fig. 20 Compared deformation between simulation and test result

Fig. 21 shows the comparison curves of E30~E120 between simulation results and test results, and values of ultimate load are summarized in Table 5. It can be seen that the overall trends of simulated curves are the same to test curves. The slope of simulated curves is slightly higher than the real situation, which is mainly due to the unclear boundary conditions of the test. The ductility showed in simulated results is low because the constitutive model used in finite element analysis is an ideal elastic-plastic constitutive model, and there is no strain hardening stage. Therefore, compared with the real situation, the displacement corresponding to peak point of simulated curves is obviously smaller. Nevertheless, the calculated values of ultimate bearing capacity and the cracking deformation agree well with the test results, which indicates that in terms of deriving strength, Hill failure criterion is suitable.

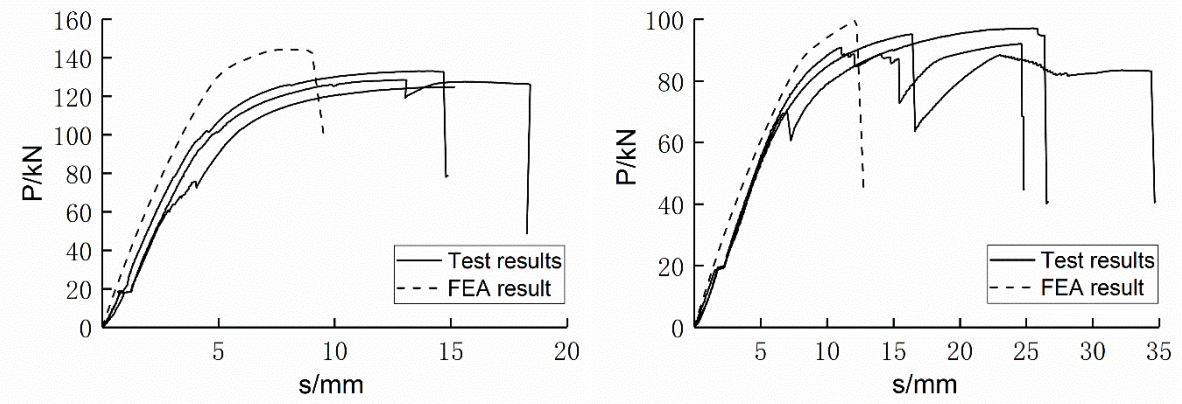

(a) E30 load vs axial displacement curves (b) E60 load vs axial displacement curves

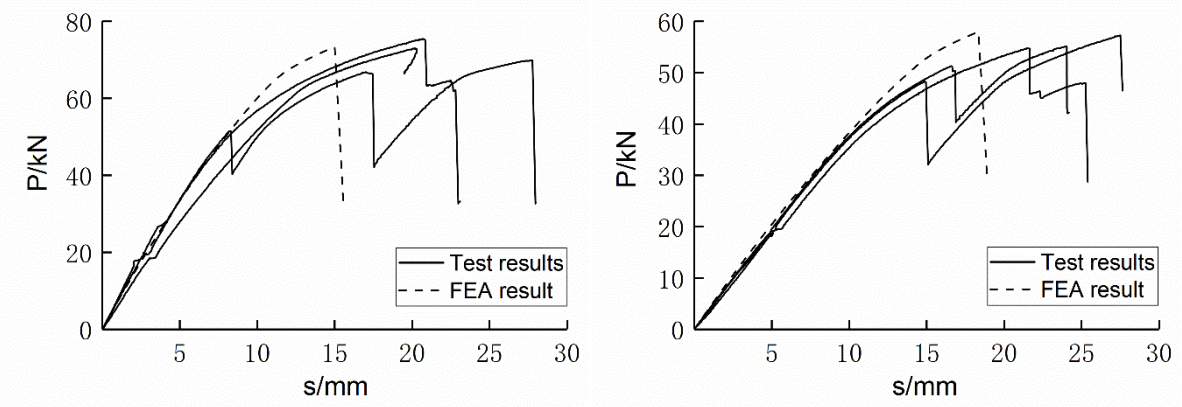

(c) E90 load vs axial displacement curves (fd E200 load vs axial displacement curves

Fig. 21 Compared curves between simulation and test

Table 5 Compared ultimate bearing capacity between simulation and test results

Group	Test results/kN	Simulation results/kN	Error/%
E30	128.89	144.3	11.96
E60	94.81	99.72	5.18
E90	72.79	73.45	0.91
E120	55.71	57.98	4.07

Note: Error = (Calculation-test) / test ×100%

4.3 General empirical formula

The above content has proved that the finite element method can effectively predict ultimate bearing capacity of LBL columns under eccentric compression. However, this method is still not convenient enough to use. In this section, a general empirical formula was proposed considering both the influence of slenderness ratio and eccentricity ratio.

In authors' previous work [37], the axial compressive behavior of LBL columns with lengths varying from 600mm to 3000mm has been studied (Fig. 22). Therefore, the finite element method is used to calculate the ultimate bearing capacity of these columns with different eccentricity ratio of 0.3, 0.6, 0.9 and 1.2. The axial compression test results and simulation results are listed in Table 6.

Fig. 22 LBL columns with different slenderness ratios

In Table 6, the stability factors are calculated by Equation (5), and the calculation formulas for slenderness ratio are:

$$\lambda = l_0 / i \tag{17}$$

$$i = \sqrt{I / A} \tag{18}$$

where l_0 is the effective length of the column, i is the radius of gyration of specimen section, I is the section moment of inertia, A is the area of cross section of the specimen.

The calculation formula for section moment of inertia of chamfered section (Fig. 23) in this paper is:

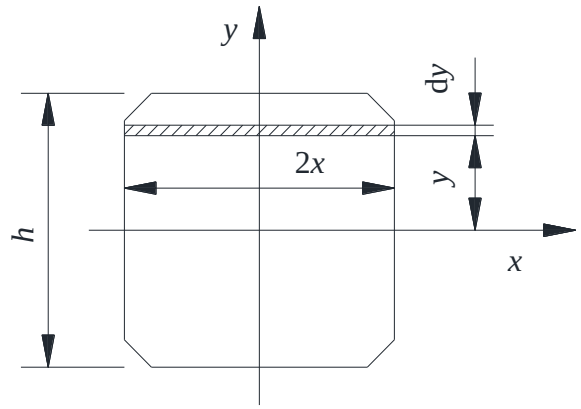

Fig. 23 Moment of inertia of the column section

$$I_x = \int_A y^2 dA = 2\int_{40}^{\frac{h}{2}} y^2 \times 2x dy + 2\int_0^{40} y^2 \times 2x dy = 4\int_{40}^{50} y^2 (90 - y) dy + 4\int_0^{40} y^2 \times 50 dy = 7.9 \times 10^6 \,\text{mm}^4 \tag{19}$$

Table 6 Test results and simulation results

L	λ	$\frac{e_0}{h}$	φ	L	λ	$\frac{e_0}{h}$	φ	L	λ	$\frac{e_0}{h}$	φ
	21.14	0	0.834		59.89	0	0.637		105.68	0	0.375
	21.14	0.3	0.341		59.89	0.3	0.143		105.68	0.3	0.086
600mm	21.14	0.6	0.220	1700mm	59.89	0.6	0.122	3000mm	105.68	0.6	0.063
	21.14	0.9	0.163		59.89	0.9	0.097		105.68	0.9	0.055
	21.14	1.2	0.128		59.89	1.2	0.080		105.68	1.2	0.049
1100mm	38.75	0	0.758	2300mm	81.02	0	0.506		—		

38.75	0.3	0.221	81.02	0.3	0.105
38.75	0.6	0.162	81.02	0.6	0.089
38.75	0.9	0.125	81.02	0.9	0.074
38.75	1.2	0.095	81.02	1.2	0.064

The correlation between stability factor, slenderness ratio and eccentricity ratio is obvious, i.e. stability factor will decrease with increase in these two factors. It can be found that the correlation can be expressed by a spatial surface (Fig. 24). The functional model is:

$$\varphi = a\lambda^{b}\exp\left(c\frac{e_0}{h}\right)+d\frac{e_0}{h}\exp\left(k\frac{e_0}{h}\right) \tag{20}$$

where φ is stability factor; λ is slenderness ratio; $\frac{e_0}{h}$ is eccentricity ratio; a, b, c, d and k are coefficients obtained through test results and simulation results.

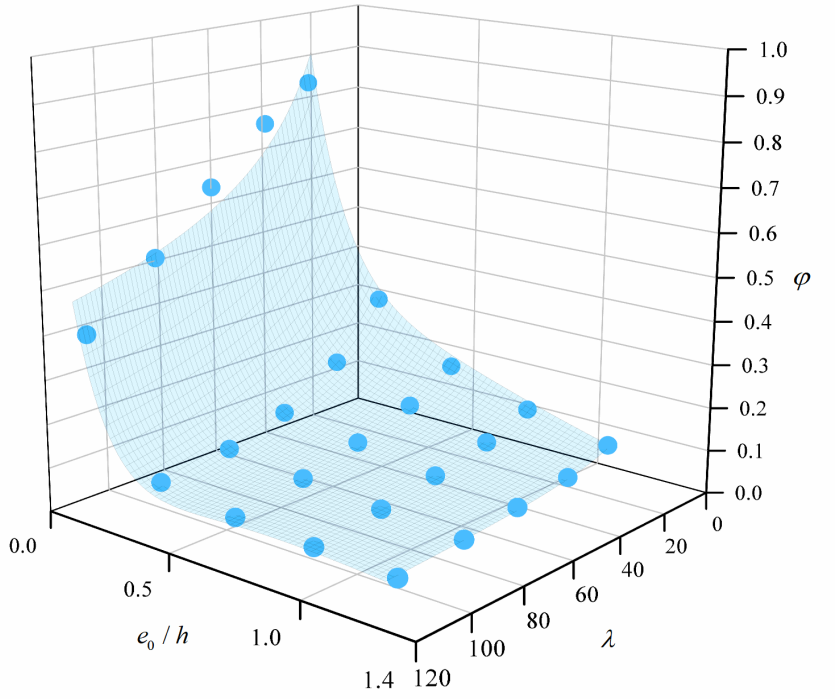

Fig. 24 Fitted spatial surface

Through regression analysis, the fitting expression is as follows:

$$\varphi = 3\lambda^{-0.4}\exp(\frac{-1.54e_0}{h})-2.56\frac{e_0}{h}\exp(\frac{-4.27e_0}{h}) \tag{21}$$

To verify the reliability of the proposed empirical formula, the test results in the existing literature and simulation results of circular-sectional column with a dimension of 100 mm × 1100 mm under tangential eccentric compression are compared with the calculated results, as shown in Fig. 25 and Table 7. The compressive strength values of laminated bamboo lumber in research [28], [29], [39] are 80.43 MPa, 80.4 MPa and 58.68MPa respectively.

The calculation formulas of section moment of inertia of rectangular section and circular section are:

$$I_{\text{rectangular}} = \frac{bh^3}{12} \tag{22}$$

$$I_{\text{circular}} = \frac{\pi d^4}{64} \tag{23}$$

where b is the width of section, h is the height of section, d is the diameter of section.

The reliability of the empirical formula can be verified as the errors between the calculated results and test results in the existing literature are basically within 20%. Besides, the simulation results of circular-sectional LBL columns also show a good agreement with the calculated results, which indicate that the empirical formula can also be used to calculate ultimate bearing capacity of LBL columns with other geometry. However, the mechanical properties of bio-based materials can be affected by parameters like moisture content, environment humidity, ambient temperature, so further experimental works and studies are required to consider more impact factors.

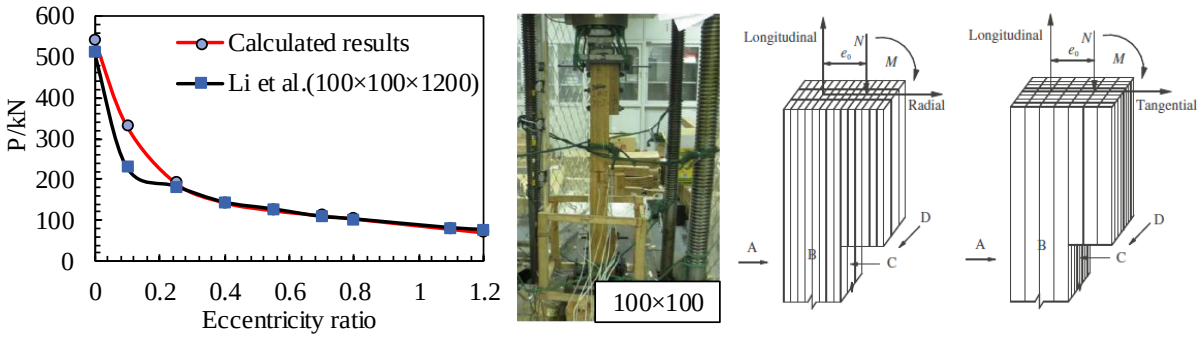

(a) Li et al. [28]

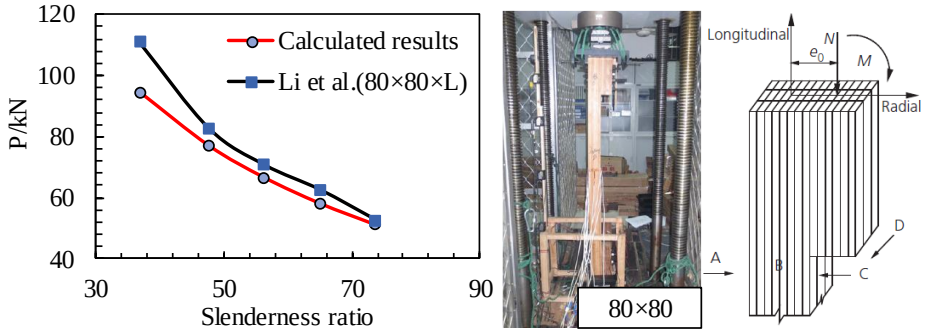

(b) Li et al. [29]

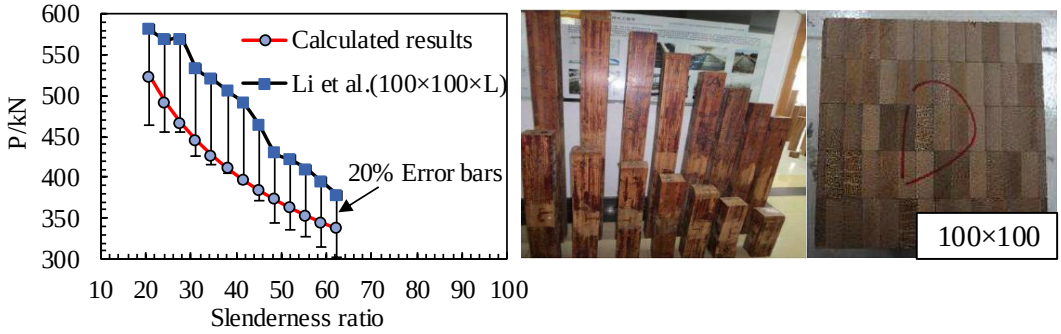

(c) Li et al. [39]

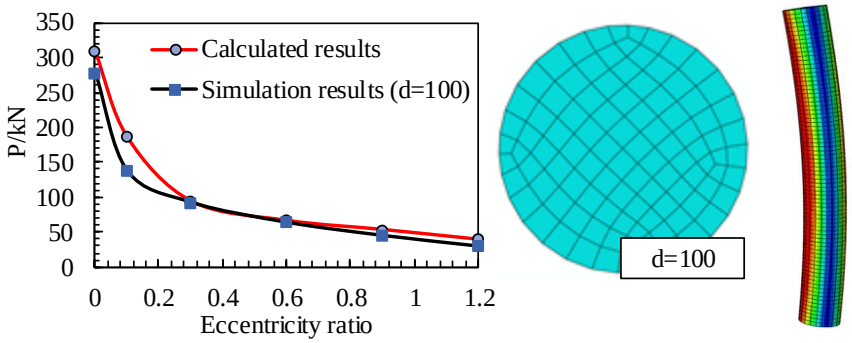

(d) LBL column with circular section

Fig. 25 Compared results

Table 7 Compared results

λ	$\frac{e_0}{h}$	P_{test} /kN	$P_{calculated}$ /kN	Error/%	λ	$\frac{e_0}{h}$	P_{test} /kN	$P_{calculated}$ /kN	Error/%
Li et al.					27.71	0	569	466.18	-18.07
41.57	0	510.8	543.28	6.36	31.17	0	533	444.73	-16.56
41.57	0.1	229.3	331.40	44.53	34.64	0	520	426.37	-18.01
41.57	0.25	182.69	192.67	5.46	38.10	0	505	410.42	-18.73
41.57	0.4	143.6	144.17	0.40	41.57	0	490	396.39	-19.11
41.57	0.55	126.81	124.74	-1.63	45.03	0	463	383.90	-17.09
41.57	0.7	108.23	112.31	3.77	48.49	0	430	372.68	-13.33
41.57	0.8	102.24	104.38	2.09	51.96	0	421	362.54	-13.89
41.57	1.1	80.47	79.18	-1.60	55.42	0	410	353.30	-13.83
41.57	1.2	76.18	70.89	-6.95	58.88	0	394	344.83	-12.48
Li et al.					62.35	0	378	337.04	-10.84
36.81	0.46	111.08	94.69	-14.75	Circular-sectional column				
47.63	0.46	82.78	77.09	-6.87	44	0	278.54	309.24	11.02
56.29	0.46	70.75	66.62	-5.84	44	0.1	138.32	186.88	35.10
64.95	0.46	62.6	58.18	-7.06	44	0.3	93.22	94.92	1.83
73.61	0.46	52.7	51.19	-2.87	44	0.6	64.66	67.25	4.00
Li et al.					44	0.9	45.94	54.21	18.00
20.78	0	580.5	523.03	-9.90					
24.25	0	568.5	491.76	-13.50					

Note: Error = (Calculation-test) / test ×100%

5 Conclusions

With different eccentricities as the influencing factors, the eccentric compression behavior and numerical study of 15 laminated bamboo lumber columns with a chamfered section were studied, and the following conclusions can be obtained:

(1) The experimental process and the ultimate failure phenomenon of columns with different eccentricities were basically consistent, which belonged to brittle tension failure. Although two defects i.e. finger joint and bamboo node were randomly distributed in the column and could affect

the initial cracking position, their effect on the overall ultimate bearing capacity could be neglected.

(2) No matter what the load levels and eccentricity of specimens were, the lateral deflection curves had similar characteristics and could be expressed by sine half wave curve. With the increase in eccentricity ratios, the ultimate bearing capacity and ultimate strain gradually decreased. The cross-section strain of specimen was basically linear distributed along the height direction, which conformed to the plane section assumption.

(3) The ABAQUS subroutine based on Hill failure criterion can effectively calculate the ultimate load of LBL columns under eccentric compression. The relative errors of the ultimate load between the simulation and the test results were less than 12%. However, due to the ideal elastic-plastic constitutive model, it cannot perfectly reflect the plastic stage i.e. the deformation of column, which resulted in much smaller ultimate axial deformation and midspan deflection values obtained from simulation.

(4) According to the simulation results and test results of LBL columns varying from 600 mm ~ 3000mm, a general empirical formula for calculating ultimate bearing capacity considering both the influence of slenderness ratio and eccentricity ratio was proposed. The formula can effectively evaluate the ultimate bearing capacity of columns under axial and eccentric compression, which was verified by comparing the test results in the existing literature and simulation results of circular-sectional column with the calculated results.

Funding: This work was supported by the National Natural Science Foundation of China (No. 51878354 & 51308301); the Natural Science Foundation of Jiangsu Province (No. BK20181402 & BK20130978); Postgraduate Research &Practice Innovation Program of Jiangsu Province; Six talent peak high-level projects of Jiang-su Province (No. JZ-029); and a Project Funded by the Priority Academic Program Development of Jiangsu Higher Education Institutions. Any research results expressed in this paper are those of the writer(s) and do not necessarily reflect the views of the foundations.

Acknowledgment: The writers gratefully acknowledge Dong Yang, Ke Zhou, Zhen Wang, Han Zhang, Hang Li, Xiaoyan Zheng, Shaoyun Zhu, Liqing Liu, Dunben Sun, Jing Cao, Yanjun Liu and others from the Nanjing Forestry University for helping with the tests.

The authors declare that they have no conflicts of interest to this work.

References

[1] Sun XF, He MJ, Li Z. Novel engineered wood and bamboo composites for structural applications: State-of-art of manufacturing technology and mechanical performance evaluation. Construction and Building Materials 2020; 249: 118751.

[2] Li X, Ashraf M, Subhani M, et al. Experimental and numerical study on bending properties of heterogeneous lamella layups in cross laminated timber using Australian Radiata Pine. Construction and Building Materials 2020; 247: 118525.

[3] Yang RY, Li HT, Lorenzo R, et al. Mechanical behaviour of steel timber composite shear connections. Construction and Building Materials 2020; 258: 119605.
[4] Chung KF, Yu WK. Mechanical properties of structural bamboo for bamboo scaffoldings. Engineering structures 2002; 24(4): 429-442.
[5] Yu WK, Chung KF, Chan SL. Column buckling of structural bamboo. Engineering Structures 2003; 25(6): 755-768.
[6] Qiu ZY, Fan HL. Nonlinear modeling of bamboo fiber reinforced composite materials. Composite Structures 2020; 244: 112240.
[7] Fei BH, Liu R, Liu XM, et al. A review of structure and characterization methods of bamboo pits. Journal of Forestry Engineering 2019; 4(02): 13-18.
[8] Huang MX, Zhang XC, Yu WJ, et al. Mechanical properties and structure characterization of bamboo softened by high temperature steam. Journal of Forestry Engineering 2016; 1(04): 64-68.
[9] Hong CK, Li HT, Lorenzo R, et al. Review on Connections for Original Bamboo Structures. Journal of Renewable Materials 2019; 7(8): 713-730.
[10] Lorenzo R, Mimendi L, Godina M, et al. Digital analysis of the geometric variability of Guadua, Moso and Oldhamii bamboo. Construction and Building Materials 2020; 236: 117535.
[11] Tian LM, Kou YF, Hao JP. Axial compressive behaviour of sprayed composite mortar–original bamboo composite columns. Construction and Building Materials 2019; 215: 726-736.
[12] Yu YL, Zhu RX, Wu BL, et al. Fabrication, material properties, and application of bamboo scrimber. Wood Science and Technology 2015; 49(1): 83-98.
[13] Zhong Y, Ren HQ, Jiang ZH. Effects of temperature on the compressive strength parallel to the grain of bamboo scrimbe. Materials 2016; 9(6): 436.
[14] Lv QF, Ding Y, Liu Y. Effect of the Nonprestressed/Prestressed BFRP Bar on Flexural Performance of the Bamboo Beam. Advances in Polymer Technology 2019; 2019(2019): 1-13.
[15] Wei Y, Zhou MQ, Zhao KP, et al. Stress–strain relationship model of glulam bamboo under axial loading. Advanced Composites Letters 2020; 29: 2633366X20958726.
[16] Li HT, Qiu ZY, Wu G, et al. Compression behaviors of parallel bamboo strand lumber under static loading. Journal of Renewable Materials 2019; 7(7): 583-600.
[17] Zhang HZ, Li HT, Corbi I, et al. AFRP influence on parallel bamboo strand lumber beams. Sensors 2018; 18(9): 2854.
[18] Li X, Ashraf M, Li HT, et al. Experimental study on the deformation and of parallel bamboo Strand Lumber under drop-weight penetration impact. Construction and Building Materials 2020; 242: 118135.
[19] Xiao Y, Wu Y, Li J, et al. An experimental study on shear strength of glubam[J]. Construction and Building Materials 2017; 150: 490-500.
[20] Wang R, Xiao Y, Li Z. Lateral loading performance of lightweight glubam shear walls. Journal of Structural Engineering 2017; 143(6): 04017020.
[21] Shan B, Xiao Y, Zhang WL, et al. Mechanical behavior of connections for glubam-concrete composite beams. Construction and Building Materials 2017; 143: 158-168.
[22] Correal JF, Ramirez F. Adhesive bond performance in glue line shear and bending for glued laminated guadua bamboo. Journal of Tropical Forest Science 2010; 2010: 433-439.
[23] Sinha A, Way D, Mlasko S. Structural performance of glued laminated bamboo beams. Journal of Structural Engineering 2014; 140(1): 04013021.
[24] Chen G, Yu YF, Li X, et al. Mechanical behavior of laminated bamboo lumber for structural application: an experimental investigation. European Journal of Wood and Wood Products 2020; 78(1): 53-63.

[25] Yang D, Li HT, Xiong ZH, et al. Mechanical Properties of Laminated Bamboo under Off-axis Compression. Composites Part A-Applied Science and Manufacturing 2020; 138: 106042.
[26] Sharma B, Gatóo A, Bock M, et al. Engineered bamboo for structural applications. Construction and Building Materials 2015; 2015 (81): 66-73.
[27] Luna P, Takeuchi C, Alvarado C, Moreno I. Glued laminated guadua angustifolia bamboo columns. Acta Hortic 2013;1003:125–30.
[28] Li HT, Wu G, Zhang QS, et al. Mechanical evaluation for laminated bamboo lumber along two eccentric compression directions. Journal of Wood Science 2016; 62(6): 503-517.
[29] Li HT, Liu R, Lorenzo R, et al. Eccentric compression properties of laminated bamboo columns with different slenderness ratios. Proceedings of the Institution of Civil Engineers–Structures and Buildings 2019; 172(5): 315-326.
[30] Karyadi, Basuki EW, Susanto PB, et al. Sidewall Thickening as Strengthening for Box-Section Laminated Bamboo Beam under Transverse Load in Shear Failure Mode. Research Journal of Applied Sciences, Engineering and Technology 2019; 16(3): 129-134.
[31] Eratodi I, Triwiyono A, Awaludin A, et al. The Effect of Specific Gravity on Embedding Strength of Glued-Laminated (Glulam) Bamboo: Numerical Analysis and Experiment. 2011.
[32] Khoshbakht N, Clouston P, Arwade S, et al. Evaluation of ASTM D5764 dowel connection tests for laminated veneer bamboo (LVB). Journal of Testing and Evaluation 2019; 47(4): 2717-2736.
[33] Tang G, Yin L, Li Z, et al. Structural behaviors of bolted connections using laminated bamboo and steel plates. Structures 2019; 20: 324-339.
[34] Hong CK, Li HT, Xiong ZH, et al. Review of connections for engineered bamboo structures. Journal of Building Engineering 2020; 2020: 101324.
[35] Wang Z, Li H, Yang D, et al. Bamboo node effect on the tensile properties of side press-laminated bamboo lumber[J]. Wood Science and Technology, 1-20.
[36] Zhang H, Li H, Hong C, et al. Size Effect on the Compressive Strength of Laminated Bamboo Lumber[J]. Journal of Materials in Civil Engineering, 2021, 33(7): 04021161.
[37] Hong C, Li H, Xiong Z, et al. Axial compressive behavior of laminated bamboo lumber columns with a chamfered section[C]//Structures. Elsevier, 2021, 33: 678-692.
[38] Hill R. A theory of the yielding and plastic flow of anisotropic metals. Proceedings Royal Society London A Mathematical, Physical Engineering Sciences 1948;193:281–97.
[39] Li H, Su J, Zhang Q, et al. Mechanical performance of laminated bamboo column under axial compression[J]. Composites part B: engineering, 2015, 79: 374-382.